Properties of ultra-thin vanadium layers in V/Ru superlattices

2007 J. Phys.: Condens. Matter 19 486005

(http://iopscience.iop.org/0953-8984/19/48/486005)

IOP PUBLISHING JOURNAL OF PHYSICS: CONDENSED MATTER

J. Phys.: Condens. Matter **19** (2007) 486005 (11pp) doi:10.1088/0953-8984/19/48/486005

Properties of ultra-thin vanadium layers in V/Ru superlattices

F Liscio[1], M Maret[1], C Meneghini[2,3], J L Hazemann[4] and M Albrecht[5]

[1] Science et Ingénierie des Matériaux et Procédés, INPGrenoble, CNRS-UJF, BP75, 38402 Saint Martin d'Hères, France
[2] Dipartimento Di Fisica, Università di Roma Tre, 00146-Roma, Italy
[3] INFM-CNR c/o ESRF, OGG GILDA Grenoble, France
[4] Institut Néel, MCMF, CNRS, BP 166, 38042 Grenoble, France
[5] Department of Physics, University of Konstanz, D-78457 Konstanz, Germany

Received 20 July 2007
Published 15 November 2007
Online at stacks.iop.org/JPhysCM/19/486005

Abstract

The properties of ultra-thin vanadium layers in V/Ru(0001) superlattices grown by molecular beam epitaxy were studied. The atomic structure of V was investigated by various methods including reflection high-energy electron diffraction (RHEED), x-ray diffraction (XRD) and polarized x-ray-absorption fine structure (PXAFS). It appears that, for up to three atomic layers, V adopts a slightly distorted hexagonal-close-packed (hcp) structure induced by pseudomorphic growth on Ru(0001). By increasing the V thickness to four atomic layers, this structure almost completely relaxes towards the body-centered-cubic (bcc) bulk structure. This sharp structural transition is also manifested in the electronic properties. A reduced superconducting transition temperature between 0.6 and 1.05 K was found in the bcc V/hcp Ru superlattice, while superconductivity is quenched in the superlattice with hexagonal V. This behavior might be linked to the existence of a ferromagnetic ground state of the metastable V induced by the hybridization of the d-bands at the hcp V/Ru interface, as predicted from first-principles density-functional theory.

1. Introduction

The development and progress of advanced material deposition techniques have resulted in an enormous increase in studies concerning the fabrication of ultra-thin films and artificial structures. In this regard, ultra-thin films can be grown pseudomorphically on suitable substrates under certain growth conditions, even when they adopt a structure different from that of bulk material. If coherent growth on a substrate is achieved, the in-plane lattice parameter of the metastable phase is constrained by interfacial interactions that favor registry with the substrate surface. Transition metals are particularly rich in metastable structures, which could be expected from the existence of various high-temperature equilibrium phases. The difference in physical properties of such metastable films compared to bulk materials has been the

key motivation for numerous studies. In particular, the magnetic properties of 3d-transition metals are predicted to change appreciably upon changing the crystal structure or interatomic distances [1–4]. Many systems have been studied, such as face-centered-cubic (fcc) Fe on Cu [5], body-centered-cubic (bcc) Co on GaAs [6], bcc Ni on Cu [7], hexagonal-close-packed (hcp) Cr on Ru [8], and Mn on GaAs [9]. In this context, V is another interesting candidate because of its large magnetic moment of 5 μ_B in its free atomic form, while bulk bcc V is paramagnetic. Experiments have shown that V grows pseudomorphically on Ni(001) up to a thickness of about eight atomic layers, revealing a body-centered-tetragonal (bct) structure with a ratio c/a close to 1.8 [10]. This bct metastable phase has also been stabilized on Cu(100) [11], however its magnetic properties have not been investigated. Recently, Zhang and Guo reported first-principles density-functional studies on the electronic and magnetic properties of V/Ru superlattices [12]. Their calculations show that two and three atomic layers of hcp V in a V/Ru superlattice exhibit ferromagnetism with a small total magnetic moment of a few tenths of μ_B. Thicker hcp V layers or V with fcc or bcc structures in V/Ru superlattices are essentially non-magnetic, revealing the importance of the stacking sequence on the formation of stable atomic magnetic moments of V in these systems.

Stimulated by the theoretical work on V/Ru superlattices [12], the growth of V on Ru(0001) and its crystalline structure in $[V(t)/Ru(10\ Å)]_{20}$ superlattices have been investigated by reflection high-energy electron diffraction (RHEED), x-ray diffraction (XRD), polarized x-ray-absorption fine structure (PXAFS), and near-edge structure (XANES) analysis. In addition, temperature-dependent ac susceptibility measurements have been performed to examine the superconducting behavior of the V/Ru superlattices, which might give an indication of the magnetic state.

2. Sample preparation

Multilayered films were prepared on $SrTiO_3(111)$ substrates by molecular beam epitaxy (MBE) in a chamber equipped with capabilities for *in situ* RHEED. The $SrTiO_3(111)$ substrates were heated to 950 K in the MBE chamber prior to deposition to remove surface contamination. Then, a 50 Å-thick epitaxial hcp Ru(0001) buffer layer was deposited at 923 K with a deposition rate of 0.1 Å s^{-1}. V and Ru layers were alternately grown at room temperature with a deposition rate of 0.1 Å s^{-1} monitored by a quartz microbalance. The pressure in the MBE chamber did not exceed 5×10^{-9} mbar during metal deposition. The compositions of the multilayers are as follows: $SrTiO_3$/Ru(50 Å)/$[V(t)$Ru(10 Å)$]_{20}$/Ru(10 Å) with a V layer thickness, t, equal to 6, 8, and 10 Å, corresponding to three, four, and five atomic V layers, respectively. A final 10 Å-thick Ru layer was included as a protective layer to prevent oxidation.

3. Experimental results and discussion

3.1. Growth of V on Ru(0001)

In situ RHEED investigations have been used to follow the growth of V on Ru(0001) at room temperature. Figure 1(a) shows RHEED patterns obtained after the deposition of 50 Å Ru on $SrTiO_3(111)$ at 923 K; the two azimuths $[10\bar{1}0]$ and $[11\bar{2}0]$ refer to the Ru(0001) surface. The patterns consist of well-defined streaks, indicating a smooth surface. In addition to the labeled fundamental hcp (0001) streaks, intermediate streaks are observed, which are a signature of a (2×2)-surface reconstruction linked to the presence of oxygen adsorbates at the surface [13]. Figure 1(b) shows the variation in the RHEED intensity of the specular beam during the V deposition. Well-pronounced RHEED intensity oscillations were observed, which characterize

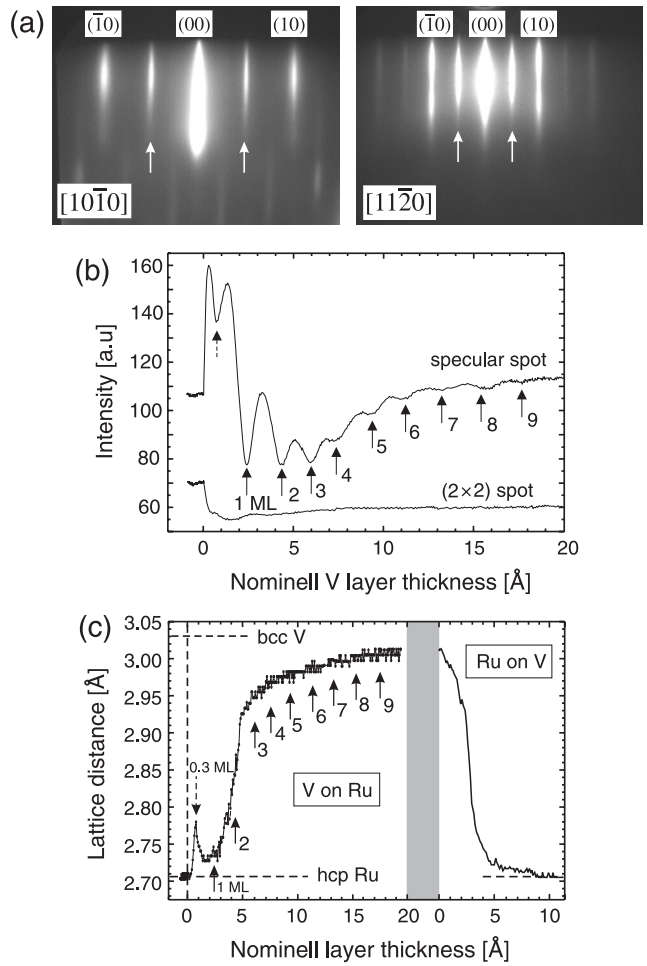

Figure 1. (a) RHEED patterns obtained after the deposition of 50 Å Ru on $SrTiO_3$(111) at 923 K, revealing a (2 × 2)-surface reconstruction. Note that the two given azimuths refer to the Ru(0001) surface. (b) RHEED intensity of the specular beam and at the reconstruction as a function of V layer thickness. (c) Variation in the in-plane lattice parameter during deposition, as extracted from the distance between the RHEED streaks recorded along the [10$\bar{1}$0] azimuth shown in (a).

a dominant layer-by-layer growth mode. Further V deposition leads to a strong damping of the oscillation, related to the transition towards a three-dimensional growth mode. Note that the reflection of the (2 × 2)-surface reconstruction vanishes immediately after the deposition of a tenth of a monolayer of V. Simultaneously, the variation in the in-plane lattice parameter during deposition, as presented in figure 1(c), was extracted from the distance between the RHEED streaks recorded along the [10$\bar{1}$0] azimuth. The Ru(0001) buffer layer was used for lattice parameter calibration, assuming an Ru in-plane lattice spacing of 2.706 Å. Figure 1(c) shows initially a peak in the lattice parameter which can be linked to the disappearance of the surface reconstruction in the submonolayer regime. Between one and four atomic layers of V, a fast relaxation of the free V surface is observed, leading to a V–V in-plane distance equal to 3.04 Å, thereby adopting the bulk bcc structure with (110) orientation analogue to the growth of Cr(110) on Ru(0001) [14]. Deposition of Ru on the almost relaxed V bcc (110) surface results

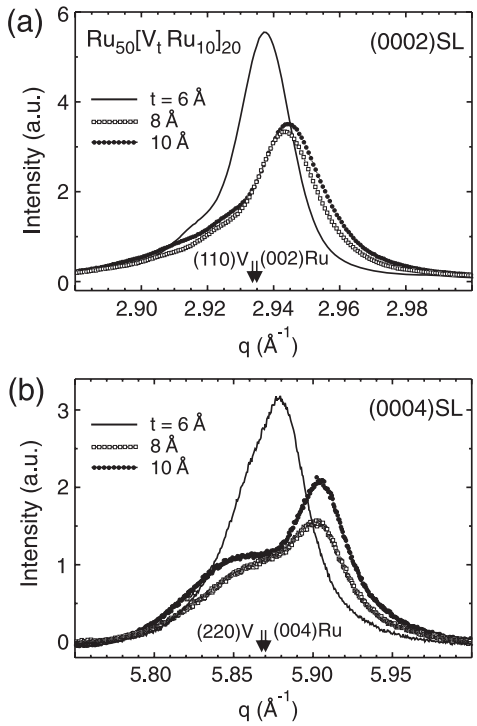

Figure 2. Series of θ–2θ scans around (a) the (0002) and (b) the (0004) SL peaks for V/Ru superlattices with various V layer thicknesses t.

in a fast relaxation process into its bulk hcp (0001) orientation which is completed after only two atomic layers of Ru. It is important to mention that the relaxation of the Ru will, in turn, affect the structural relaxation of the buried V layers by inducing an additional compressive stress at the V–Ru interface.

3.2. Structural properties of V/Ru superlattices

3.2.1. X-ray diffraction. X-ray diffraction patterns were recorded on a Siemens D5000 diffractometer using a Cu Kα source. Figure 2(a) shows a series of θ–2θ scans around the (0002) peak for V/Ru superlattices with various V layer thicknesses. The x-ray patterns are presented as a function of the scattering vector, $q = \frac{4\pi \sin(\theta)}{\lambda}$, and, for comparison, the vectors corresponding to the (110) and (0002) reflecting planes of V and Ru bulk phases, respectively, are marked. By increasing the V thickness, a shift towards higher q-values and a broadening of the Bragg peak of the superlattice (SL) is observed. For t equal to 6 Å, the rather narrow Bragg peak of the SL whose position is close to the bulk (0002) Ru and bulk (110) V positions indicates uniform stacking of atomic planes along the growth direction. From its full width at half maximum (FWHM), a coherence length $L_\perp$ can be extracted which is very close to the total superlattice thickness. For t equal to 8 and 10 Å, the intensity of the (0002) SL peak is significantly reduced and the two peaks appear most likely to be related to the Ru buffer layer and mainly distorted V and Ru in the multilayer. These two contributions can be better separated around the (0004) higher-order peak, as shown in figure 2(b). The positions of the (0004) SL peak correspond to spacings between planes parallel to the surface averaged through the multilayer. For $t = 6$ Å the average spacing is equal to 2.138 Å; assuming a spacing of

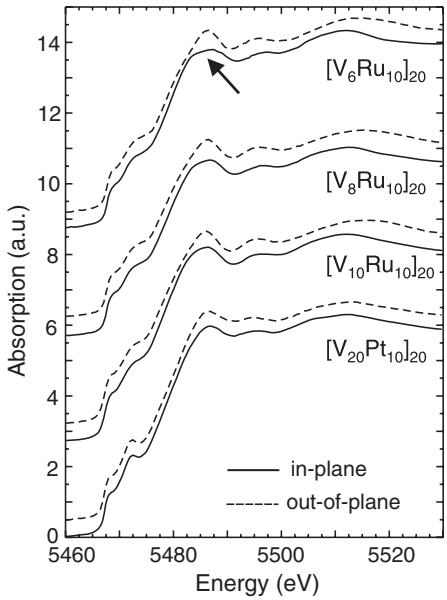

Figure 3. V K-XANES spectra of V/Ru and V/Pt multilayers measured for in-plane (solid lines) and out-of-plane (dashed lines) polarizations. A pronounced polarization dependence for the thinner multilayers is observed. The curves are normalized to unity for clarify.

the Ru 0002 planes equal to that in bulk Ru (2.1408 Å), the spacing of the V planes is equal to 2.135 Å. For $t = 8$ or 10 Å, the spacing is equal to 2.129 Å, which is significantly smaller than the spacing of the (110) bcc V planes (2.1413 Å) and (0002) hcp Ru planes. The FWHM of the (0004) SL peak for $t = 8$ and 10 Å leads to a coherence length of about 75% of the total superlattice thickness. This can be related to the two different stacking sequences through the V and Ru layers, which prevent constructive interference.

From the RHEED observations and x-ray measurements, it is suggested that V layers of up to three atomic planes can be stabilized in a metastable hexagonal structure, but a further increase in the thickness from four to five atomic layers results in a relaxation of the V layer stack into a distorted bcc (110) bulk structure. It is worth noting that a different behavior was found for Cr/Ru superlattices, where a gradual relaxation towards its bcc bulk structure with increasing Cr thickness was observed [14]. Due to the closeness of the interplanar distances of the (110) V and (0002) Ru planes, it is important to corroborate the structural change by other techniques. In the next subsection, we present the results extracted from x-ray absorption spectroscopy (XAS) measurements.

3.2.2. X-ray absorption spectroscopy. XAS measurements were performed at the V K-edge on the CRG-BM32 beamline at the European Synchrotron Radiation Facility (ESRF) in Grenoble, France. Absorption spectra were collected at room temperature in total electron yield mode. For each V/Ru superlattice, two spectra were collected with beam polarization in the film plane ($\parallel$ polarization) and out of the film plane ($\perp$ polarization). Note that the samples were kept rotating around the normal to the surface during data collection to avoid the Bragg peaks of the substrate [15].

Figure 3 shows the XANES regions of the spectra for the three V/Ru superlattices and for a [V(20 Å)Pt(10 Å)]$_{20}$ multilayer used as a reference for the bcc V structure. For the V/Pt

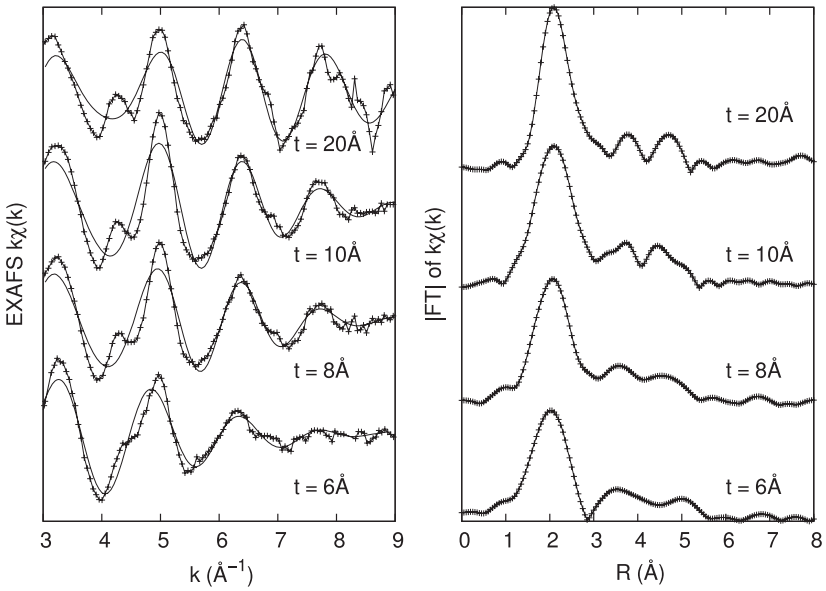

Figure 4. Experimental (crosses) and filtered (solid lines) signals of the out-of-plane EXAFS data (left-hand panel) and modulus of the Fourier transforms of the $k\chi(k)$ spectra (right-hand panel) obtained for the V/Ru superlattices for various V layer thicknesses t. The V-XAFS spectrum of a $[V_{20}Pt_{10}]_{20}$ multilayer (for $t = 20$ Å) is shown for comparison.

sample, the XAS signal is independent on polarization, as expected for a cubic lattice [16]. For V/Ru superlattices the polarization dependence of the XANES spectra is well pronounced for $t = 6$ Å and decreases progressively when the V layer thickness increases. While the single out-of-plane XANES peak remains unchanged, the enhancement in splitting of the in-plane XANES peak around 5485 eV is a signature of a structural transition from bcc to hcp as the V layer thickness decreases.

Although the XANES spectra are useful for probing a global structural change, their quantitative analysis requires complex full multiple scattering calculations [17], which is outside the scope of this work. In contrast, analysis of the extended region (EXAFS) [18] is a current and easier way to extract quantitative structural information. The experimental XAS spectra, $\mu(E)$, were treated following standard methods to extract the EXAFS signal $\chi(k)$: the pre-edge background was fitted with a straight line and subtracted; the post-edge atomic background, i.e. the atomic absorption, was modeled with a smooth polynomial spline through the experimental data. The scale for the photoelectron wavevector ($k = \hbar^{-1}\sqrt{2m_e(E - E_0)}$, where m_e is the electron mass) was defined, taking the origin of the photoelectron energy at 5475 eV.

Figure 4 shows the out-of-plane EXAFS spectra for the V/Ru and V/Pt multilayers and their k-weighted Fourier transforms (FT). The first peak of the FTs at around 2 Å contains the contributions of the nearest neighbors. As the V thickness decreases, the first peak decreases and variations occur in the next-neighbor region ($R > 3$ Å). The quantitative analysis of the EXAFS spectra is performed by fitting the k-weighted experimental data $k\chi(k)$, employing the standard EXAFS formula [19]:

$$k\chi_{\text{th}}(k) = S_0^2 \sum_j \frac{N_j}{R_j^2} F_j(k) \exp(-2k^2\sigma_j^2) \exp\left(-\frac{2R_j}{\lambda(k)}\right) \sin(2kR_j + \phi_j(k)), \quad (1)$$

Table 1. Interatomic distance R_j, and out-of-plane and in-plane coordination numbers, $N_j^{\perp}$ and $N_j^{\parallel}$, around an atom located in a (110) bcc plane and an atom in a (0001) hcp plane; effective coordination numbers of out-of-plane and in-plane neighbors, $\widetilde{N}_j^{\perp}$ and $\widetilde{N}_j^{\parallel}$, using out-of-plane and in-plane polarization geometries.

Structural parameters			Out-of-plane polarization		In-plane polarization	
R_j	$N_j^{\perp}$	$N_j^{\parallel}$	$\widetilde{N}_j^{\perp}$	$\widetilde{N}_j^{\parallel}$	$\widetilde{N}_j^{\perp}$	$\widetilde{N}_j^{\parallel}$
bcc phase						
$\frac{\sqrt{3}}{2}a^{\mathrm{bcc}}$	4	4	7.88	0.12	2	6
a^{bcc}	4	2	5.94	0.06	3	3
hcp phase						
a^{hcp}[a]	6	6	11.8	0.2	3	9

[a] When $c/a \neq 1.63$, the out-of-plane nearest-neighbor distance is equal to $\sqrt{\frac{a^2}{3} + \frac{c^2}{4}}$.

where N_j is the multiplicity of the jth contribution, and $2R_j$ and σ_j^2 are, respectively, the average absorber-to-neighbor distance and the relative mean square displacement (Debye–Waller factor). $F_j(k)$ and $\phi_j(k)$ are the amplitude and phase-shift functions. $\lambda(k)$ is the photoelectron mean free path and S_0^2 is an empirical parameter, taking into account losses due to many-body effects. Dealing with a non-isotropic structure, an effective multiplicity number, $\widetilde{N}_j$, has to be used instead of N_j. The $\widetilde{N}_j$ takes into account the polarization dependence of the photo-absorption process and single scattering processes. It is given by

$$\widetilde{N}_j = 3\sum_{i=1}^{N_j} \cos^2 \alpha_{ji}, \tag{2}$$

where α_{ji} is the angle between the x-ray polarization vector and the bond direction between the absorbing atom and the ith scatterer in the jth shell.

For the two beam polarizations, the contributions of the in-plane and out-of-plane nearest-neighbor atoms to $\widetilde{N}_j$ are summarized in table 1 for the bcc and hcp structures. For the bcc structure, the nearest-neighbor shell consists of two close subshells: one with eight neighbors at $R_{\mathrm{I}}^{\mathrm{bcc}} = a^{\mathrm{bcc}}\sqrt{3}/2$, four in the (110) plane ($N^{\parallel}$) and four out-of-plane ($N^{\perp}$) (two above and two below the plane); and the other subshell with six neighbors at $R_{\mathrm{II}}^{\mathrm{bcc}} = a^{\mathrm{bcc}}$, two in the (110) plane ($N^{\parallel}$) and four ($N^{\perp}$) out-of-plane (two above and two below the plane). For the hcp structure the nearest-neighbor shell consists of 12 neighbors at $R^{\mathrm{hcp}} = a^{\mathrm{hcp}}$: six in the plane and six out-of-plane (three above and three below the plane). The effective coordination numbers in the two structures are reported in table 1. For out-of-plane polarization, only the out-of-plane atoms contribute to the signal, while for in-plane polarization both in-plane and out-of-plane atoms contribute to the XAFS signal. As previously reported for Cr/Ru multilayers [14], we limited our analysis to the out-of-plane nearest-neighbor filtered spectra, which allows discrimination between the two possible structures of the V layers. The filtered signal are calculated by inverse Fourier transform of the first peak of the FT, extended between 1 and 3 Å. The filtered signals for the different superlattices are superimposed on the experimental XAFS spectra presented in figure 4.

For the different nearest-neighbor shells and for single scattering, the amplitudes and the phase shifts were calculated using the FEFF code [20] for the two possible structures of V layers using the parameters reported in table 2. For V hcp the lattice parameter c is taken to be equal to twice the spacing of the (110) planes in bcc V and the lattice parameter a is calculated assuming a ratio c/a that is identical to that of hcp Ru. To calculate the amplitude of Ru and the phase shift of the V–Ru pairs in the first-neighbor shell of the V hcp stacking, the three

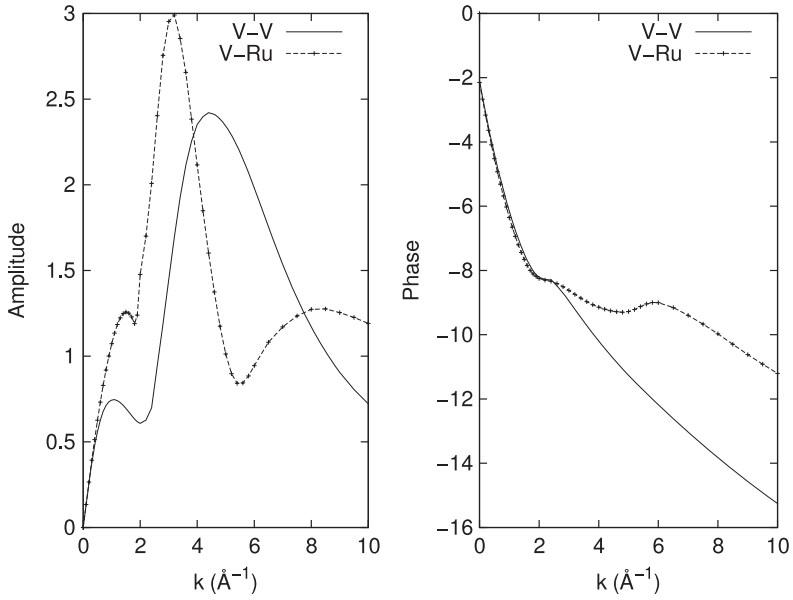

Figure 5. Amplitudes and phases of SS signals for V–V and V–Ru atomic pairs (also see the text).

Table 2. Volumes and lattice constants of the unit cells for bcc V, hcp V, and hcp Ru. Please note that the (110) interatomic distance in bcc V is very close to the (0001) interatomic distance in hcp Ru.

	V_{bcc}	V_{hcp}	Ru_{hcp}
Vol (Å^3)	13.884	13.579	13.53
a (Å)	3.0282	2.7039	2.7057
c (Å)		4.2817	4.2816
	$c^{hcp} \approx \sqrt{2}a^{bcc}$		
	$(c/a)V_{hcp} \approx (c/a)Ru_{hcp}$		

V first neighbors located in the (0001) plane just above the plane containing the central atom are replaced by three Ru atoms. As shown in figure 5 for hcp V layers, V and Ru neighbors give rise to different amplitudes and total phase shifts. In particular, the contribution of V–Ru pairs is larger for k-values below 4 Å^{-1} and the total phase shifts provide strong differences for $k > 3$ Å^{-1}. Note that, for bcc V layers, the backscattering amplitude of V atoms at a distance of $a^{bcc}\sqrt{3}/2$ is similar to that of V nearest neighbors in an hcp environment and that the amplitude of the V atoms at a distance a has the same k-dependence but a lower intensity level. Moreover, the total phase shifts for the two V–V pairs are very close to that for hcp V.

To minimize the number of refined parameters and the correlations among them, the coordination numbers were fixed to the values deduced from the number of V atomic planes in each V layer and from the type of stacking sequence, neglecting the small contribution of the in-plane neighbors as mentioned in table 1. Moreover, the V–Ru distance extracted from the simulation of the filtered signal for $[V_6Ru_{10}]_{20}$ is kept constant in fitting the two other filtered spectra ($t = 8, 10$ Å), and the two distances for the bcc V layers are correlated with a ratio equal to $\frac{\sqrt{3}}{2}$. Figure 6 shows the best fits obtained for the two possible atomic structures of the V layers. It appears that, in addition to the V–Ru shell, the superlattice with $t = 6$ Å

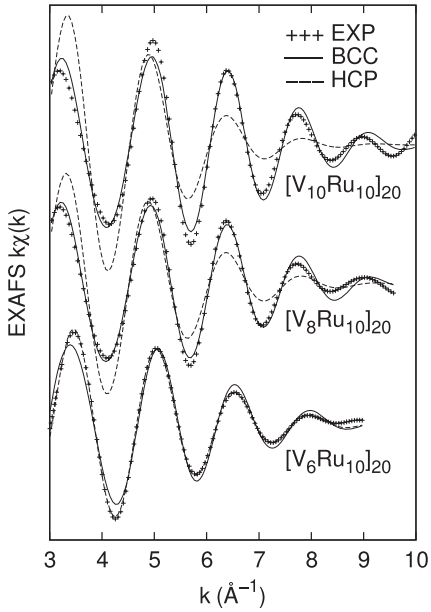

Figure 6. Experimental data (+) and corresponding theoretical fit assuming a bcc V (solid lines) and an hcp V structure (dashed lines) using the out-of-plane filtered EXAFS signals.

Table 3. Structural parameters extracted from the best fits of the out-of-plane filtered XAFS spectra in V/Ru superlattices as a function of V layers thickness. The parameters in bold characters are kept fixed in fitting the filtered spectra. Errors on the last digit are included.

	First out-of-plane V neighbors			First out-of-plane Ru neighbors		
t (Å)	R_j (Å)	$\widetilde{N}_j$	σ_j (Å)	R_j (Å)	$\widetilde{N}_j$	σ_j (Å)
6	2.55(3)	**8**	0.16(3)	2.65(3)	**4**	0.21(3)
8	2.58(3)	**6**	0.13(3)	**2.65**	**3**	0.22(3)
	2.97(5)	**4.5**	0.14(5)			
10	2.59(3)	**6.4**	0.13(4)	**2.65**	**2.4**	0.22(3)
	2.98(3)	**4.75**	0.12(8)			

is already well represented by a single V–V shell in an hcp environment, while, including a second V–V subshell (by assuming a bcc environment), the quality of the fit becomes worse. In contrast, for t equal to 8 and 10 Å, the fits are definitely better using two V–V subshells, confirming the bcc structure of the V layers with more than three atomic planes. The structural parameters extracted from the best fits are reported in table 3. For $t = 6$ Å, the V–Ru distance equal to the nearest distance in hcp bulk Ru is larger than the V–V distance in the hcp V layers, indicating a more compact stacking in the hcp V layers. Based on a c lattice parameter of hcp V equal to 4.27 Å (the value extracted from x-ray data), this first V–V distance would lead to a lattice parameter a equal to 2.415 Å, i.e. much smaller than that measured from the RHEED pattern, equal to 2.95 Å. As already observed for the Cr/Ru superlattices [8], XAFS is sensitive to the smallest distances, therefore a value of a equal to 2.415 Å is underestimated. For $t = 8$ and 10 Å, the first two distances V–V are shorter than those in bcc V bulk (2.6225, 3.028 Å). These deviations are in agreement with the x-ray data, which have shown a shift of the (0004)SL position towards the larger q-values with respect to the (220) V position. For

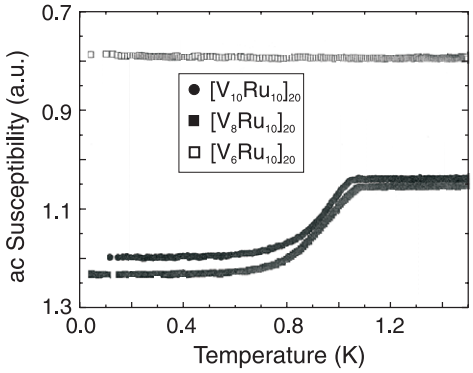

Figure 7. Temperature dependence of the ac susceptibility χ' for various V/Ru superlattices. Measurements were performed down to 20 mK.

the three superlattices, the σ_j values for the V–Ru pairs are larger than those of the V–V pairs, reflecting some disorder at the V/Ru interfaces.

Summarizing the experimental results on the structural properties, it has been shown that ultra-thin V layers with a thickness of three atomic layers reveal a hexagonal structure with a lattice parameter c equal to 4.27 Å (close to that of hcp Ru) and a lattice parameter a close to 2.95 Å based on the RHEED patterns. Larger V thicknesses result in a transition into a bcc (110) stacking which, from x-ray and XAFS data, is denser than in the bulk.

3.3. Electronic properties of V/Ru superlattices

The difference in electronic energy which accompanies a structural phase change is often of the same order of magnitude as the energy associated with a magnetic phase change, leading to a close correlation between structure and magnetism, particularly in 3d-transition metals [21]. While magnetic investigations are rather difficult to interpret due to the small amount of V, we have investigated the electronic properties of V/Ru superlattices at low temperatures. The ac susceptibility is the standard nondestructive method for the determination and characterization of superconductors, in particular for measuring the critical temperature. Experimentally, the real part of the susceptibility, χ', is observed to be stepwise a function of temperature, representing a transition from near-perfect screening to complete penetration of the external ac magnetic field into the sample, while the peak observed in the imaginary part of the susceptibility, χ'', is a measure of dissipation in the sample. The temperature dependence of ac susceptibility was measured for an ac field of 50 Oe perpendicular to the film plane at a frequency of 1 kHz. Figure 7 shows the temperature dependence of the ac susceptibility, χ', for various V/Ru superlattices. A reduced superconducting transition temperature between 0.6 and 1.05 K was found in the bcc V/hcp Ru superlattices. In this case, it is well known that bcc V and hcp Ru exhibit, respectively, transition temperatures of 5.3 and 0.49 K in bulk samples [22] and that this transition temperature is expected to be modified due to the proximity effect in ultra-thin superlattices [23]. However, the superlattice with hexagonal V does not show any indication of a superconducting state down to a temperature of 20 mK, the experimental limit of the setup. It is suggested that this might be an indication of the existence of a ferromagnetic state in V induced by hybridization of the d-bands at the hcp V/Ru interfaces, as predicted from first-principles density-functional theory [12]. However, further studies are required to verify this suggestion.

4. Summary

In summary, V/Ru superlattices have been fabricated by molecular beam epitaxy on Ru(0001). The growth and structural properties were analyzed by *in situ* RHEED, XRD and x-ray absorption spectroscopy. It has been shown that ultra-thin V layers with a thickness of up to three atomic layers can be stabilized in a slightly distorted hexagonal structure. A further increase in the V thickness from three to four atomic layers results instantaneously in a transition of the whole V layer stack into its bcc (110) bulk structure. This sharp structural transition is also manifested in the electronic properties. A reduced transition temperature between 0.6 and 1.05 K was found in the bcc V/hcp Ru superlattices, while, for the superlattice with hexagonal V, no normal–superconducting transition was found down to 20 mK. The quenching of the superconductivity might be an indication of the existence of ferromagnetic V, as predicted from first-principles density-functional theory for hcp V/Ru heterostructures [12]. However, the metastable phase of V is certainly accompanied by a strong modification of the electronic band structure, which in turn will influence the superconductivity as well.

Acknowledgments

The authors would like to thank E Döring for fruitful discussions. Financial support was provided by the Deutsche Forschungsgemeinschaft through the Emmy–Noether program and SFB 513 at the University of Konstanz.

References

[1] Papaconstantopoulos D A, Fry J L and Brener N E 1989 *Phys. Rev.* B **39** 2526
[2] Marcus P M, Qiu S L and Moruzzi V L 1999 *J. Phys.: Condens. Matter* **11** 5709
[3] Moruzzi V L 1986 *Phys. Rev. Lett.* **57** 2211
[4] Moruzzi V L and Marcus P M 1989 *Solid State Commun.* **71** 203
[5] Keune W, Holbauer R, Gonser U, Lauer J and Williamson D L 1977 *J. Appl. Phys.* **48** 2976
[6] Prinz G A 1985 *Phys. Rev. Lett.* **54** 1051
[7] Schulz B and Baberschke K 1994 *Phys. Rev.* B **50** 13467
[8] Albrecht M, Maret M, Köhler J, Gilles B, Poinsot R, Hazemann J L, Tonnerre J M, Teodorescu C and Bucher E 2000 *Phys. Rev. Lett.* **85** 5344
[9] Zhang S B, Zhang L, Xu L, Wang E G, Liu X, Jia J-F and Xue Q-K 2004 *Phys. Rev.* B **69** 121308(R)
[10] Tian Y, Jona F and Marcus P M 1998 *Phys. Rev.* B **58** 14051
[11] Tian Y, Jona F and Marcus P M 1999 *Phys. Rev.* B **59** 12286
[12] Zhang T and Guo G Y 2005 *Phys. Rev.* B **71** 214442
[13] Albrecht M, Köhler J, Friemelt K and Bucher E 1998 *Surf. Sci.* **415** 170
[14] Albrecht M, Maret M, Köhler J, Gilles B, Poinsot R, Hazemann J L, Tonnerre J M, Teodorescu C and Bucher E 2002 *Phys. Rev.* B **66** 205410
[15] Revenant-Brizard C, Regnard J R, Mimault J, Duclos D and Faix J J 1997 *J. Physique* IV **7** C2325
[16] Maret M, Bley F, Meneghini C, Albrecht M, Köhler J, Bucher E and Hazemann J L 2005 *J. Phys.: Condens. Matter* **17** 2529
[17] Natoli C R, Benfatto M and Doniach S 1986 *Phys. Rev.* A **34** 4682
[18] Rehr J J and Albers R C 2000 *Rev. Mod. Phys.* **72** 621
[19] Lee P A, Citrin P H, Eisenberger P and Kinkaid B M 1981 *Rev. Mod. Phys.* **53** 769
[20] Zabinsky S I, Rehr J J, Ankudinov A, Albers R C and Eller M J 1995 *Phys. Rev.* B **52** 2995
[21] Prinz G A 1991 *J. Magn. Magn. Mater.* **100** 469
[22] Bückel W 1984 *Supraleitung* (Weinheim: Physik Verlag)
[23] Hübener M, Tikhonov D, Garifullin I A, Westerholt K and Zabel H 2002 *J. Phys.: Condens. Matter* **14** 8687